THE GEOLOGICAL SOCIETY
OF AMERICA

Chapter 2.3

Fractures in welded tuff

Kenneth Wohletz

Los Alamos National Laboratory, Los Alamos, New Mexico 87545, USA

INTRODUCTION

A notable feature and, in many cases, a distinguishing aspect of welded tuff is the occurrence of numerous fractures. These fractures, generally oriented in a nearly vertical fashion, are rather equally spaced, and show little or no displacement. Produced by cooling and contraction perpendicular to isotherms in tuff after its emplacement and during its welding, these fractures are often referred to as *cooling joints*, resembling columnar joints developed in basaltic lava flows. Notable exceptions are where joints form plumose patterns in fumarolic zones. These fractures play a dominant role in the structural integrity of welded tuffs, their hydrology, and, by secondary processes, their mineralogy.

The Bandelier Tuff of New Mexico provides field data that illustrate fracture characteristics. Erupted 1.13 million years ago, the upper member of the Bandelier Tuff (Tshirege Member) is well exposed in numerous canyons that cut the Pajarito Plateau in northern New Mexico. It displays prominent fractures, which likely play an important role in the vadose-zone hydrology of the tuff and the surface manifestations of the tectonic fabric. Detailed canyon wall maps, discussed here, record the location and morphology of over 5000 fractures, represented in nearly 8 km of canyon-wall exposure. Being best developed in more strongly-welded zones, fractures extend from the surface of the tuff to the pumice fallout underlying it. The average fracture spacing is 1.5 m in studied locations giving a linear density of 65 fractures per hundred meters. Notable increases in fracture density up to 230 per hundred meters occur over tectonic lineaments associated with the Pajarito fault system. Fracture strikes are widely dispersed, but do show a crude bimodal distribution that defines a conjugate system of northwesterly- and northeasterly-oriented fracture sets. Since fracture maps represent vertical cross sections along generally west-to-east canyon walls, a fracture set generally paralleling these canyons is not well documented, but its presence is indicated by simple trigonometric approximations.

Rare surface exposures of fracture sets show a polygonal, often rhombohedral, pattern, though in places the pattern is nearly orthogonal or hexahedral. Most fractures are steeply dipping (~80°), but nearly horizontal fractures are also evident. They display both planar (constant aperture) and sinuous (variable aperture) surfaces, averaging 0.7–1.0 cm aperture in all studied areas; fractures in tectonic zones, however, show average apertures up to 5 cm. Although most fractures are not filled at depth, they are packed with detritus and secondary minerals within about 15 m of the surface. Combining linear density and fracture aperture data shows that an average of 0.7 m of total aperture exists over any 100-m interval, but it can rise to over 5 m of total aperture per hundred meters over tectonic zones.

An interesting result of this characterization is a demonstration of how a fractured-welded tuff can conceal faults by accommodating strain incrementally in each fracture over a wide area. Calculations based on the fracture data indicate that the Bandelier Tuff conceals fault displacement of up to several meters. The occurrence and distribution of fractures in welded tuff is an important consideration for slope stability and infiltration of surface water and contaminants. The development of new dual-porosity/dual-permeability numerical procedures for predicting contaminant dispersal relies on accurate input of fracture characteristics. Providing obvious pathways for dispersal, the Bandelier Tuff shows that fracture fillings of detrital materials and secondary minerals actually block migration along fractures near the tuff's surface. At deeper levels, fractures make the tuff very permeable and capable of containing large quantities of water.

BACKGROUND

Most fractures in welded tuff can be attributed to what is most widely known as columnar jointing, a textural feature displayed by generally vertical, evenly spaced cracks that intersect to form polygonal columns. These fractures are in many ways similar to

5- and 6-sided columnar joints formed in basaltic lava flows. Ross and Smith (1961) attributed columnar jointing in welded tuffs to cooling tension, but noted that the columns more frequently form rectilinear joint sets. Since that study there has been little work on characterizing these joints until hydrogeologic studies of welded tuffs started at the Nevada Test Site (NTS) in the 1970s. Barton and Larsen (1985) studied NTS joint fracture patterns in order to better understand water infiltration and movement in the vadose zone. They suggested a fractal nature to the occurrence of these fractures. More recently Fuller and Sharp (1992) characterized tuff fractures and their hydrologic properties with a detailed characterization of fracture spacing and orientation, combined with an analysis of fracture permeability.

This chapter reviews welded tuff fractures, their origins, characteristics, and possible significance. Table 2.3.1 outlines the ranges of welded tuff physical properties and shows that most notable variations (e.g., permeability) are linked to the degree of welding.

The columnar joints that produce fractures in welded tuffs are illustrated by example photographs shown in Figures 2.3.1 through 2.3.4. While nearly vertical orientations are most common, highly slanted and radiating distribution of joints are typical for tuffs that have cooled over irregular topography or have been modified by fumarolic activity. The occurrence of joints in welded tuffs is summarized by the schematic illustration shown in Figure 2.3.5.

Because most fractures in welded tuffs are manifestations of columnar jointing, characterization is achieved by measurement

TABLE 2.3.1. WELDED TUFF PHYSICAL PROPERTIES

Property	Minimum	Maximum
Bulk Density (Mg/m^3)[a]		
Nonwelded	0.5	1.8
Partially welded	1.8	2.0
Moderately welded	2.0	2.3
Densely welded	2.3	2.6
Median grain size (mm)	0.06	8
Porosity	0	0.6
Permeability (m^2)		
Nonwelded	1 x 10^{-17}	1 x 10^{-12}
Welded	1 x 10^{-19}	1 x 10^{-16}
Young's Modulus (E, Mb)	0.04	0.14
Shear Modulus (Mb)	0.02	0.6
Poisson's Ratio (ν)	0.10	0.15
Crushing strength (kb)	1.3	1.3
Cohesive strength (kb)	0.3	0.3
Compressional velocity (km/s)	0.7	4.6
Shear velocity (km/s)	0.8	2.0
Heat capacity (kJ/kg-K)[b]	1.0	1.2
Conductivity (W/m-k)	0.2	0.4
Electrical resistivity (Ω-m)		
Nonwelded	17	60
Welded	200	1400

[a] Bulk densities are dependent upon composition; density generally decreases with increasing silica content.
[b] Heat capacities for nonporous tuff can be multiplied by porosity to get effective heat capacity.
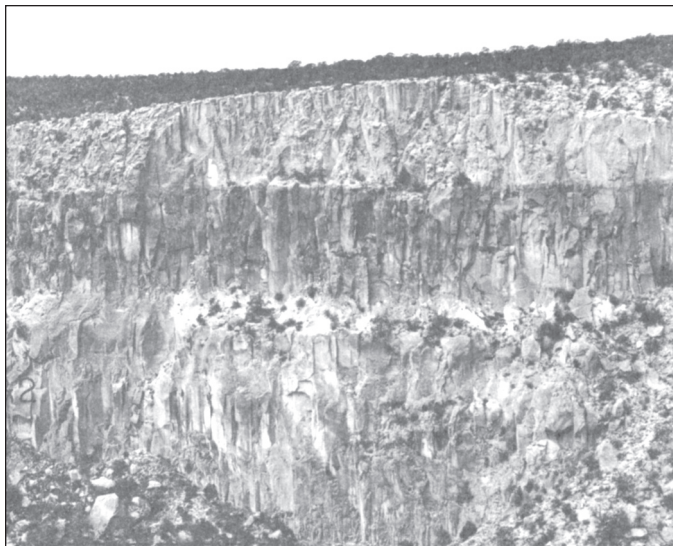
Figure 2.3.1. The Bandelier Tuff in Frijoles Canyon of northern New Mexico. Note the darker-colored, strongly welded zone near the top of the canyon wall where fractures are best displayed.

Figure 2.3.2. The Bandelier Tuff in Los Alamos Canyon showing orthogonal columns averaging ~0.5–1.0 m on a side. These columns spall from the cliff face during canyon sidewall erosion, which occurs most readily where fractures are most closely spaced.
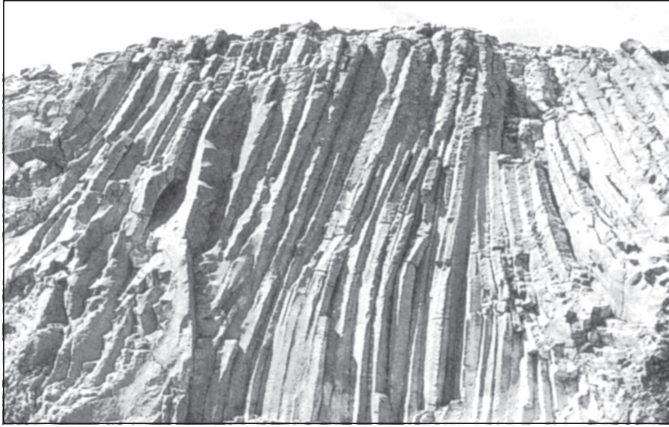
Figure 2.3.3. Columnar jointing in the outflow facies of the Cerro Galan ignimbrite of northwest Argentina. The cliff face is ~20 m high and shows a marked curvature of the joint pattern from vertical, likely a reflection of bowed isotherms that existed in the tuff during cooling. Photograph was adapted from Francis (1993).
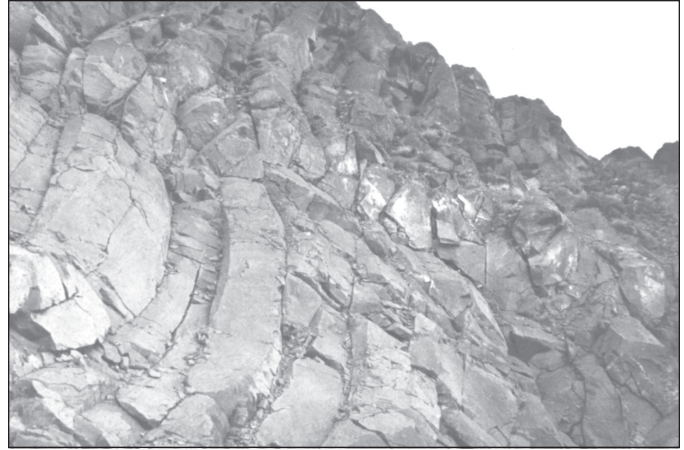
Figure 2.3.4. Strongly curved columnar joints in the densely welded zone of the Bishop Tuff in eastern California that radiate away from a fumarolic pipe. The joints are spaced by ~1 m. Photograph was adapted from Fisher and Schmincke (1984).

of joint spacing, orientation, and aperture. This type of characterization will be described and analyzed in this paper.

Joint Formation Model

A model for joint formation can be formulated based upon the hypothesis that jointing results from volumetric contraction and vertical compaction during tuff cooling and welding. This contraction and compaction leads to growth of in situ stresses that concentrate in excess of rock moduli. Because of their similarity to columnar joints in basaltic lavas, the model of DeGraff and Aydin (1993) should also apply to joint formation in welded tuffs. In that model, joints grow away from a cooling surface normal to maximum tensile stress.

With welding compaction, one may assume that the upper and lower surfaces of the tuff are free to contract vertically. In contrast, lateral contraction and bending of the tuff are mechanically constrained, which leads to horizontal stress buildup. The stress dissipation is strongly coupled to temperature-dependent rheology. For example, where the tuff is ductile, stresses are accommodated by viscous flow, but where it is brittle, an elastic response to stress builds up. Assuming that the brittle-ductile transition temperature (T_s) is abrupt and dependent on composition (T_s = 725–1065 °C), and rock below T_s is linearly elastic, fractures form in brittle regions and terminate where $T > T_s$ at which point the tuff responds in a ductile fashion. Because heat loss is dominantly from the bottom and top surfaces of the tuff, isotherms are horizontal where the substrate is horizontal, such that
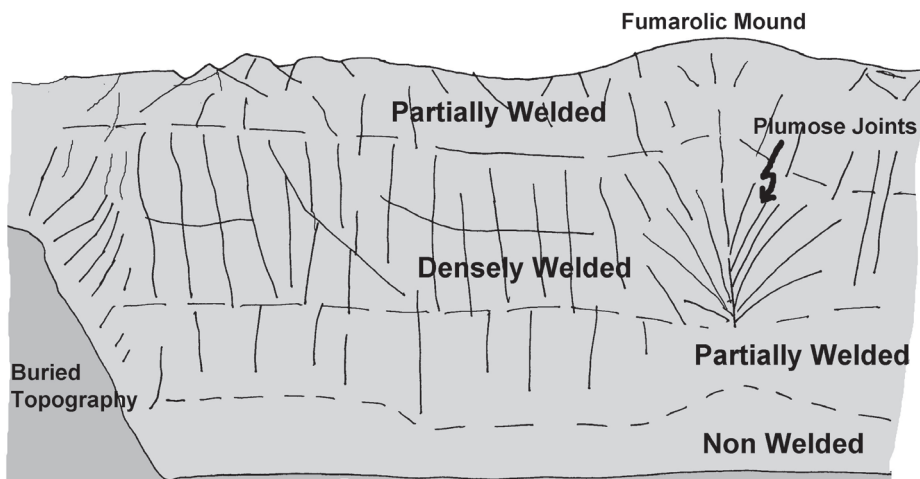
Figure 2.3.5. Schematic representation showing the distribution of columnar jointing in a welded tuff. Most closely spaced in the densely welded zone, a few of the joints are continuous into the partially welded zones above and below, but generally do not extend downward into the nonwelded zone. Joints generally grow parallel to the cooling gradient of the tuff and thus are perpendicular to cooling surfaces. Most commonly vertical, joints may grow at moderate angles from vertical near buried topography. Where vertical heat flow is concentrated along fumarolic pipes within the tuff, joints tend to radiate outward, forming a plumose pattern. Secondary mineralization associated with fumarolic activity commonly makes tuffs more resistant to erosion so that fossil fumaroles are manifested as mounds on the surface of tuffs.

$$T(z) = T_0 + (T_s - T_0)\left(\frac{z}{z_s}\right),$$

for the upper portion of the tuff, where T is temperature (subscripts s and 0 denote solidus and ambient temperatures, respectively), z is depth, and z_s is the depth of the brittle-ductile transition. The simple, conductive, model-dependent stress distribution (vertical stress neglected and horizontal stresses equal) shows a variation dependent upon depth:

$$\sigma_x = \sigma_y = \frac{\alpha E(T_s - T_0)}{1 - v}\left(1 - \frac{z}{z_s}\right),$$

where horizontal stresses are denoted by σ_x and σ_y, α is the thermal expansion coefficient, E is Young's modulus, and v is Poisson's ratio. Because the horizontal stresses are positive, the tuff is in tension. This cooling and stress magnitude structure is illustrated in Figure 2.3.6.

For the elastic chilled region, deformation leads to stress buildup and concentration at discontinuities (e.g., lithic fragments) where fractures nucleate. Fractures tend to elongate incrementally when stress concentration at a fracture tip (denoted by K_I, which is the stress intensity factor) increases above fracture toughness (K_c). With each incremental fracture growth, stress concentration is temporally relieved only to build up again with further cooling.

For a joint that is uniformly loaded, the stress intensity factor is commonly expressed (Lawn and Wilshaw, 1975) as:

$$K_I = 1.2\sigma_x\sqrt{\pi c},$$

where c is the fracture length. The fracture toughness is typically in the range of 1–4 MPa m$^{1/2}$. This incremental growth model is illustrated in Figure 2.3.7.

This model of joint growth predicts a growth increment dependent upon joint spacing. For the case when a is equal to the joint half length, and b is the horizontal half-spacing, Figure 2.3.8 shows the relationship of growth increment (c/a) to normalized joint spacing as a function of the overall reduction in the fracture tip stress concentration. Overall, when applied to a tuff overlying a nearly horizontal substrate, this model predicts vertically oriented joints (hence fractures) with spacing that tends to decrease
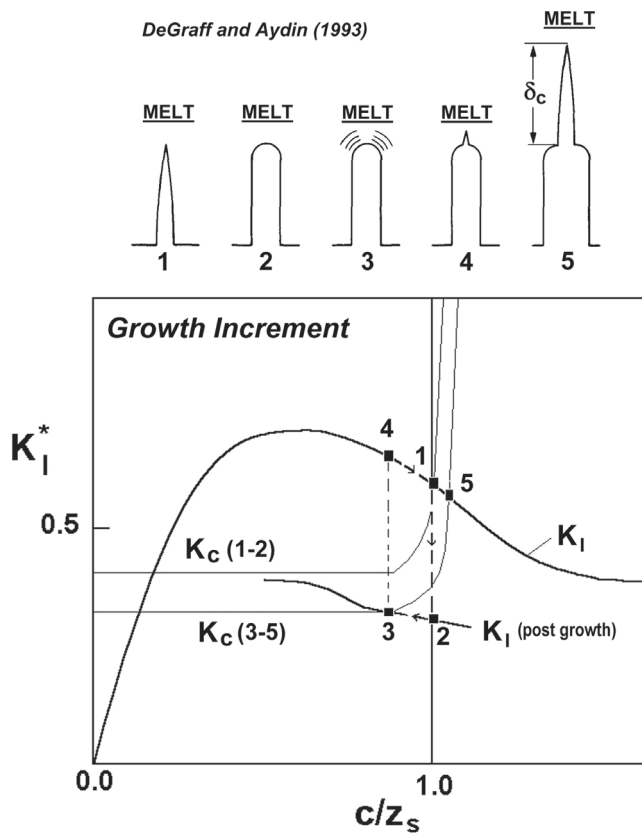
Figure 2.3.7. Plot adapted from DeGraff and Aydin (1993) showing five stages of the incremental growth of a columnar joint fracture into cooling tuff. K_I^* is the normalized stress intensity factor, and K_c is thermally dependent fracture toughness. K_I^* is shown as a function of c/z_s, the ratio of fracture length to depth of the solidus isotherm, which decreases constantly with cooling but increases abruptly with incremental growth. With deformation near or within viscous tuff (1) ($T \geq T_s$), the fracture tip becomes blunted (2), then cooling causes the solidus surface to move away from the blunted fracture, causing stress to build up (3) and eventually concentrate into a sharp tip (4), where K_I^* is greater than K_c, leading to incremental growth δ_c (5).

Figure 2.3.6. A plot adapted from DeGraff and Aydin (1993) showing the thermal profile (T) at some initial time ($t = 0$) and the prefracture stress magnitude as a function of depth (z). In this model, horizontal stresses (σ_x) are greater than vertical stress, the bottom and top portions of the tuff are chilled and brittle, but the central portion (below a depth of z_s) is still viscoplastic.

as cooling rate increases. Such a prediction indicates that thicker welded tuffs will tend to have more widely spaced joints than thinner tuffs, if cooling is dominantly conductive.

FRACTURE CHARACTERISTICS

Detailed fracture investigations of the upper member of the Bandelier Tuff of northern New Mexico (Vaniman and Wohletz, 1990; Kolbe et al., 1995; Vaniman and Chipera, 1995; Walters, 1996; Reneau and Vaniman, 1998; Wohletz, 1995a, 1995b, 1996, 1998) provide data that illustrate the distribution and character of fractures in welded tuff. Figure 2.3.9 shows a geological map of the central portion of Los Alamos National Laboratory, which is situated on the Pajarito Plateau. The upper member of the Bandelier Tuff is subdivided into four units of varying degrees of welding (Fig. 2.3.10). Incision by west-to-east–running canyons exposes cliff sections of the tuff, which has allowed detailed fracture mapping. Seven horizontal transects have been
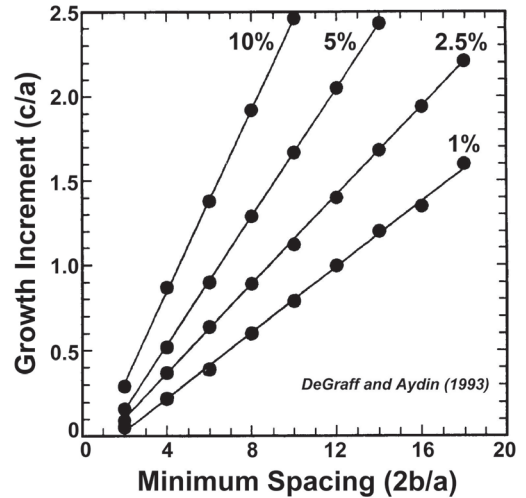
Figure 2.3.8. From DeGraff and Aydin (1993), this plot shows that where joints are more widely spaced with respect to their half length, the growth increment will be larger. Solutions are shown for a range of overall joint tip stress intensity decrease due to growth. Where more stress is relieved during growth, the growth increment will be larger.
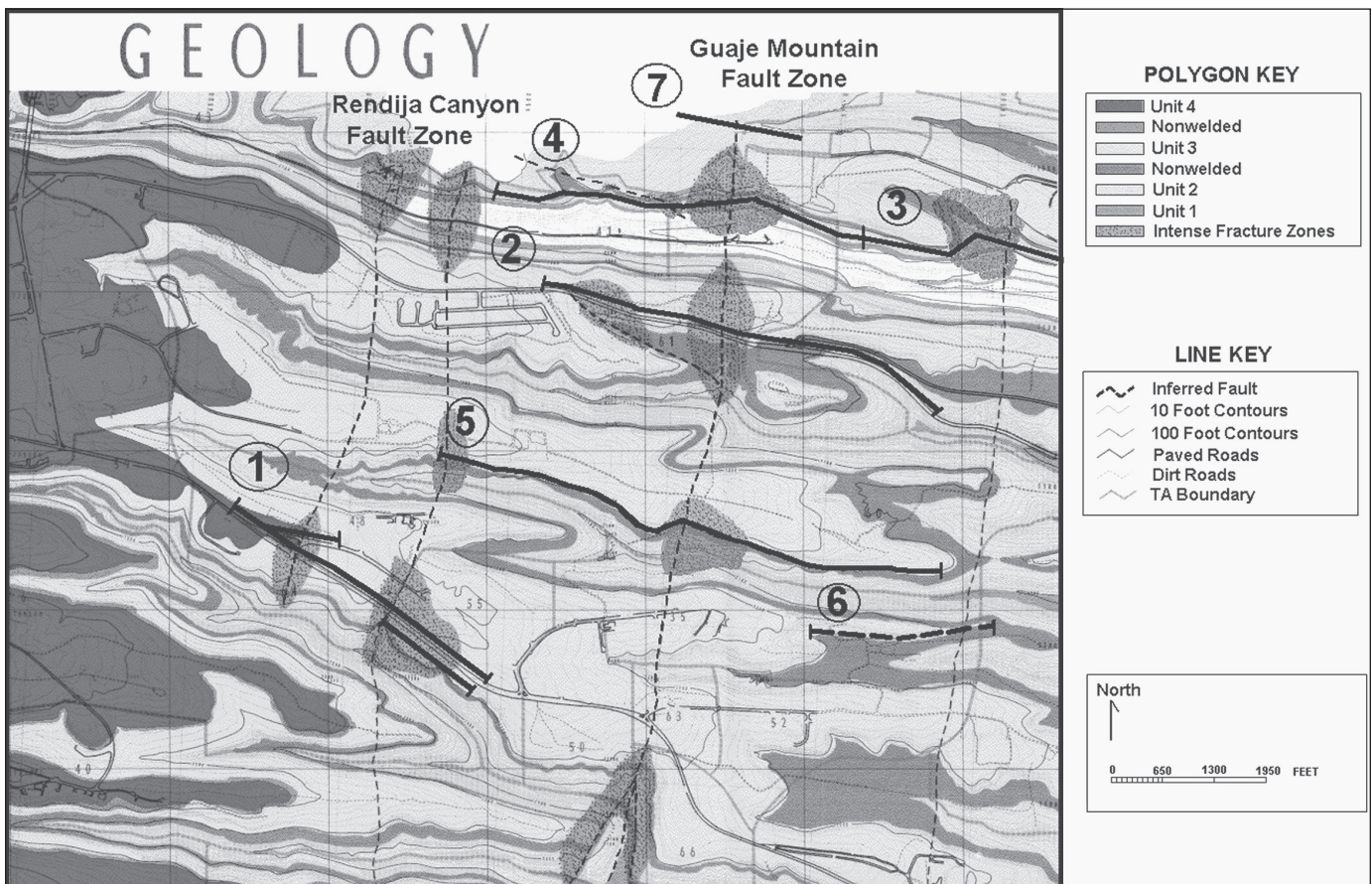
Figure 2.3.9. Geological map of the central part of Los Alamos National Laboratory area on the Pajarito Plateau (adapted from Vaniman and Wohletz, 1993). Bandelier Tuff units are shown in blues, greens, yellows, and red. Brown stippled areas are zones of intense fracturing, mostly along mapped traces of the Rendija Canyon fault and Guaje Mountain fault. Seven fracture transects are shown: (1) along the north side of Two Mile Canyon; (2) along the north side of Sandia Canyon; (3) lower Los Alamos Canyon; (4) upper Los Alamos Canyon; (5) Mortandad Canyon, (6) the north side of Acid Canyon; and (7) just north of Los Alamos Canyon.
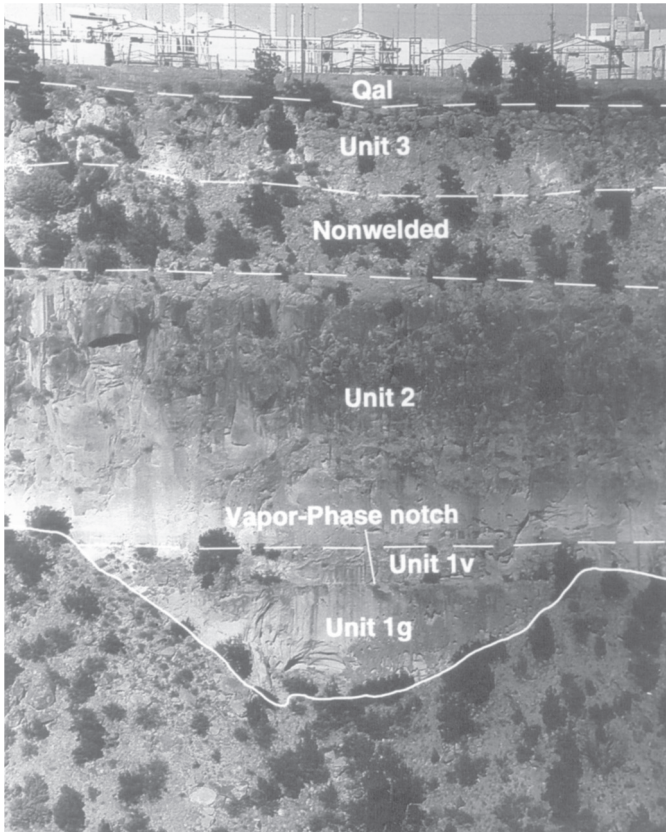
Figure 2.3.10. Photograph of the northern cliff face of Los Alamos Canyon near DP Mesa. From bottom to top, the stratigraphy of the tuff includes nonwelded Unit 1, partially covered by Quaternary talus and consisting of glassy and vapor-phase altered portions. Unit 2 is moderately welded and overlain by a nonwelded transition into Unit 3 (partially welded), which is in turn overlain by Quaternary alluvium. Note that Unit 4 has been presumably removed by erosion in this area.

investigated, generally running along the northern slopes of canyons where fractures are best exposed. Because these mapped transects cross two major fault zones (Rendija Canyon fault zone and Guaje Mountain fault zone), the investigations revealed the relationship of cooling joint fractures to fractures possibly caused by tectonic movement.

The method of investigation involved creation of photomosaics along the canyon walls to serve as base maps for fracture mapping (Fig. 2.3.11). The photographs were taken so that most fractures could be readily identified. Each fracture was assigned a number, and for each, several characteristics were systematically measured and added to a database for later analysis. The best exposures of fractures were noted in Unit 2 and Unit 3, and most fractures could be traced through both units. Because the investigation methods applied to environmental efforts using engineering plans with distance measured in feet, the distance unit is retained in the following sections.

The results of this study, summarized in the following sections, show that fracture density (spacing) averages 20/100 ft, frac-

ture strikes are apparently controlled by local stress patterns that existed on the Pajarito Plateau during and after tuff emplacement, fracture dips are generally vertical, fracture apertures average ~1 cm, and fracture fillings exist mainly within 15 m of the surface and are derived from infiltrated clay and calcite derived from soil. As discussed later in this paper, cooling fracture characteristics are intimately tied to tectonic displacement that occurred both before and after the tuff emplacement, cooling, and compaction.

Fracture Density

Fracture density was calculated as the number of fractures in 100 ft intervals centered on each fracture. Average fracture spacing was found to be fairly constant over all areas of investigation at ~5 ft (20/100 ft) in studied areas, but over tectonic zones, the fracture density exceeded values of >60/100 ft (Fig. 2.3.12). This marked increase of fracture linear density over tectonic zones is not readily apparent from outcrop observations. As shown in Figure 2.3.12, the density variation expressed as number of fractures in 10 ft intervals centered on each fracture is small, generally unrecognizable to the eye and only readily apparent from data plots representing density over 100 ft intervals. However, in regions outside studied areas where the thickness of welded units is about one-third of that for the measured transects, average fracture spacing does decrease to ~2 ft, which supports the predictions of the joint formation model.

Fracture Strike

In general, variability in fracture strike causes vertical fractures to intersect and form polygonal columns. Many fractures are sinuous, showing curvature in strike. Fracture strikes show a crude polymodality in distribution (Table 2.3.2), which for the E-W profiles documented can be characterized as NW- and NE-trending fracture sets, but an E-W set is theoretically extant (Fig. 2.3.13). Because N-S exposure is extremely limited, as is mesa-top fracture exposure, it is difficult to prove the calculated distribution shown in Figure 2.3.13. The calculations do show a fracture distribution that produces 60° intersections, which perhaps fits tensional fracture of an isotropic brittle material better. Because most fractures are either part of the NW- or NE-trending sets, fracture intersection produce 4-sided columns that have orthogonal to rhombic angles. Fractures tend to be orthogonal over fault zones and are slightly rotated eastward (Fig. 2.3.14). Figure 2.3.15 is a three-dimensional projection of fractures measured along an E-W section. Although the calculated N-S cross section does not show a marked dominance of E-W–trending fractures, it qualitatively shows that where fractures are more closely spaced, they tend to intersect at lower angles—the larger fracture-bounded blocks tend to be more orthogonal.

Fracture Dip

Most fractures tend to be nearly vertical, although more horizontally oriented ones tend to form along planes that mark changes
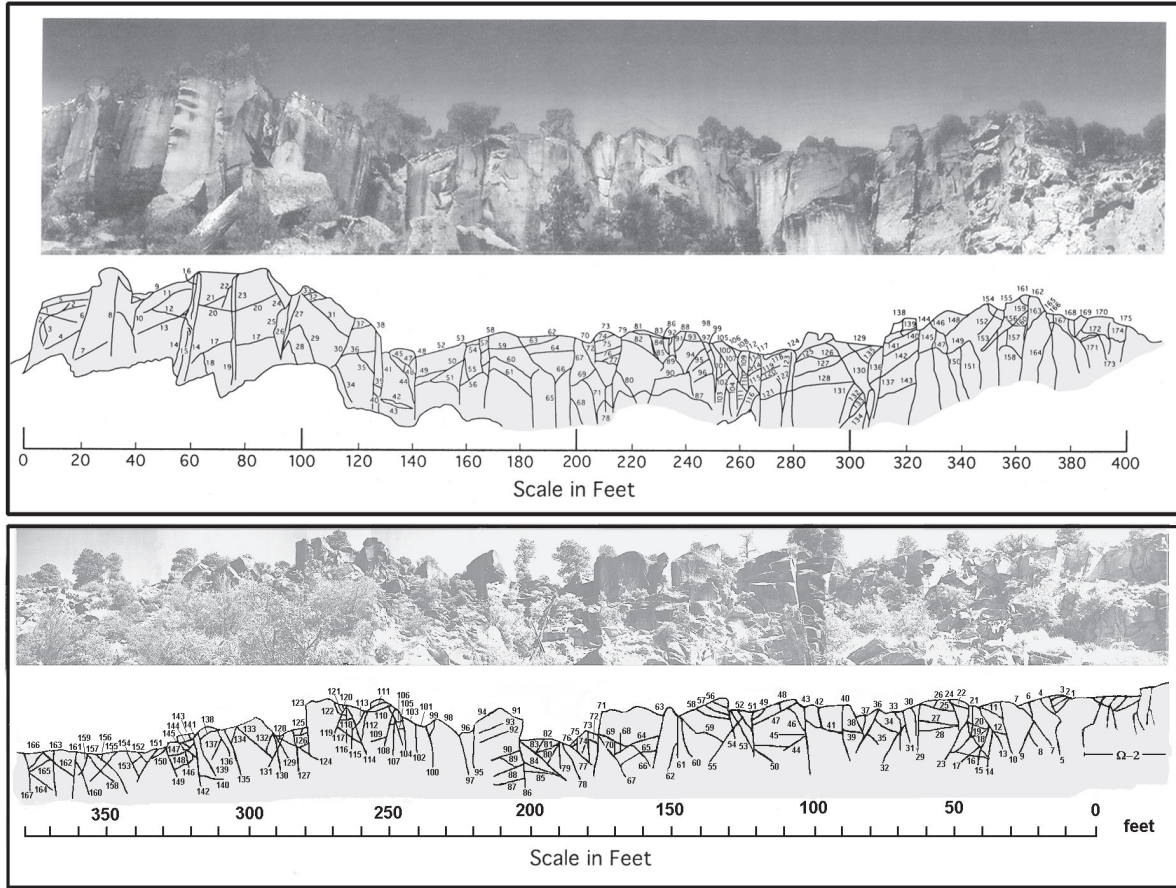
Figure 2.3.11. Examples of two fracture maps for Los Alamos Canyon, the top one depicting an area where fractures are well exposed by a cliff face, and the bottom one, a region where fractures are poorly exposed.

in tuff properties (e.g., welding). Most fractures are sinuous in dip, but a few are very planar. Table 2.3.3 shows that the average dip is from 70° to 80°, and that there is little variation of dip between strike sets (NW and NE), between background fractures and those in a fault zone, and between northerly and southerly dipping fractures. An observation true for the Bandelier Tuff is that measured dips along canyon walls tend to be in a direction away from the canyon walls. This observation may stem from the likelihood that fractures dipping toward the canyon are more likely to spall during sidewall erosion and thus are not preserved. Figure 2.3.16 shows variation of fracture dip angle for all fractures, northerly, and southerly dipping fracture sets. Note that over the fault zone, fractures become less steep, and the angle between northerly and southerly dipping fractures tends to grow large. However, from Table 2.3.3, it is apparent that the fault zone is not readily apparent from dip variation on the NE and NW fracture sets.

Aperture

Fractures show variable aperture because of fracture sinuosity, as described above in fracture dip characteristics explanation.

TABLE 2.3.2. FRACTURE STRIKE DATA

Fracture Set	Number	Mean Strike	Standard deviation
All Fractures	4940	N9E	±46
NE	2820	N44E	±25
NW	2120	N36W	±25
Background (west)	1085	N5E	±46
NE	557	N44E	±26
NW	528	N35W	±22
Fault zone	933	N10E	±50
NE	527	N47E	±24
NW	406	N39W	±25
Background (east)	1297	N13E	±48
NE	756	N43E	±24
NW	541	N30W	±22
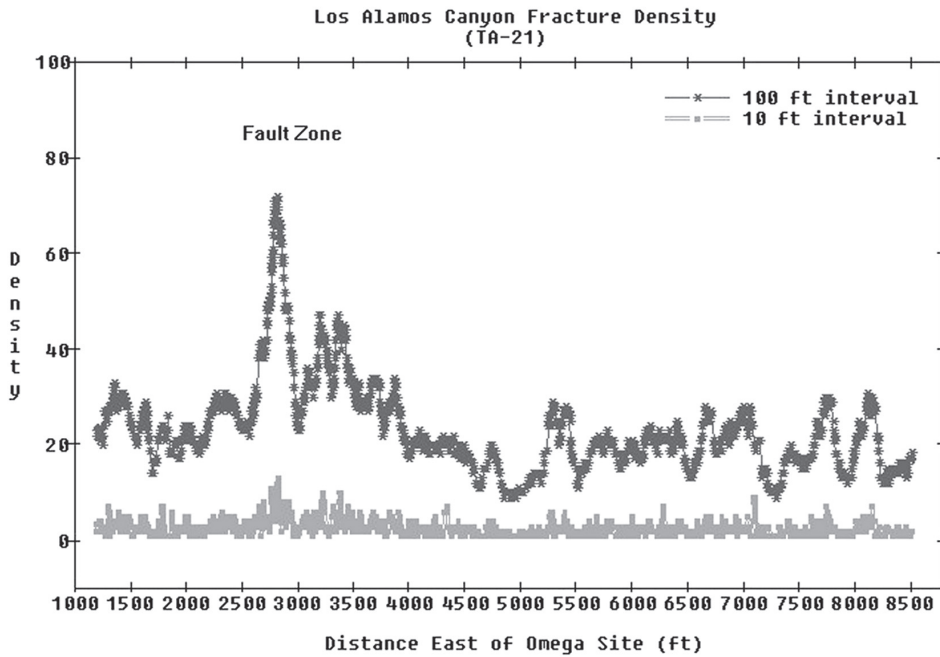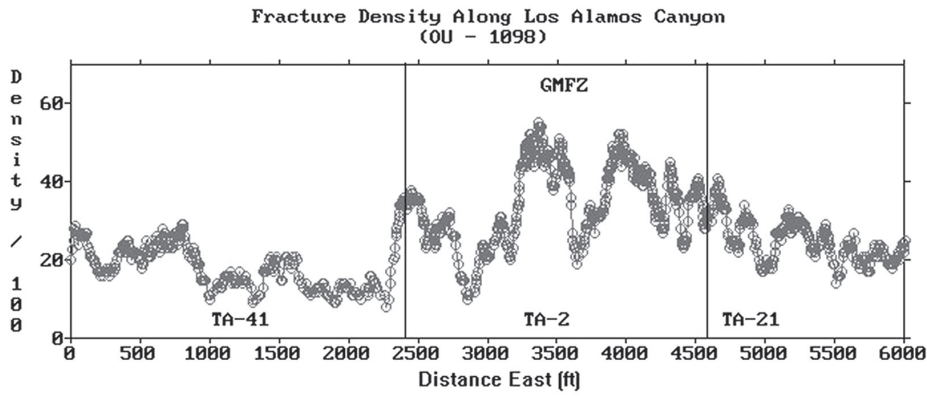
Figure 2.3.12. Two examples of fracture density measurements. The top plot displays fracture density that increases near Omega site where the Guaje Mountain fault zone extends. The bottom plot shows measurements of densities under Material Disposal Area V (MDA-V). The bottom curve in the lower plot shows density calculated as the number of fractures per 10 ft interval, which is more what a field observer would perceive, perhaps masking the larger-scale trends.
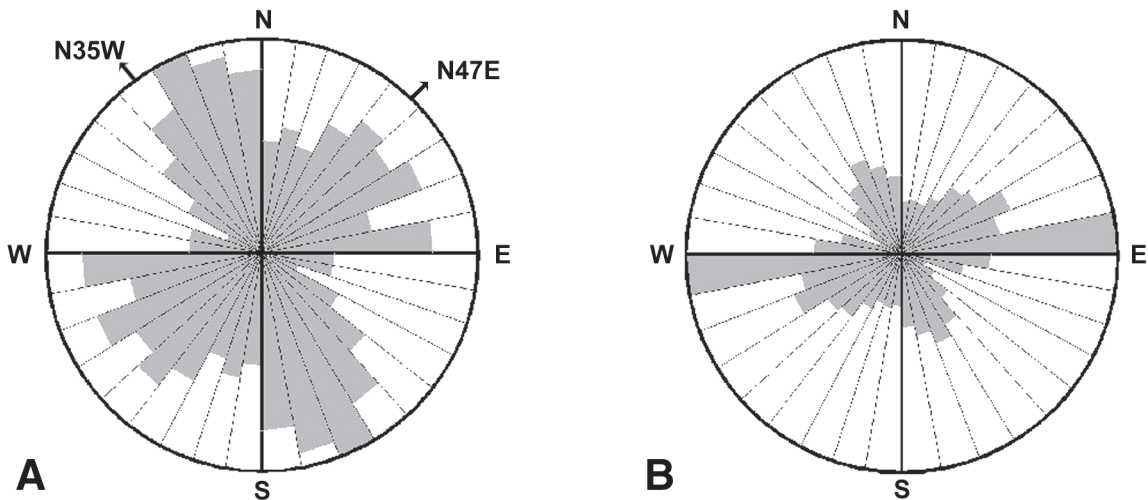
Figure 2.3.13. Fracture strike distributions. (A) Measured (apparent) distribution showing two modes characterizing NW- and NE-trending fracture sets. Because fractures were observed along a generally E-W transect, fractures parallel to this transect are not well exposed. By calculating the effect of geometry on exposure, a hypothetical distribution (B) shows that in fact E-W–trending fractures may dominate.
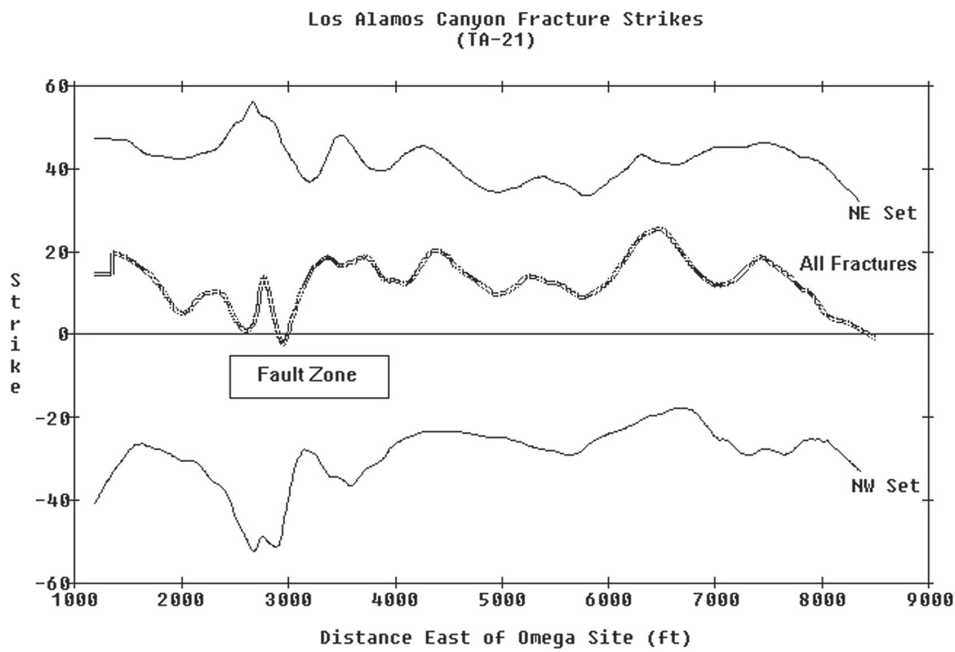
Los Alamos Canyon Fracture Strikes
(TA-21)

NE Set
All Fractures

Fault Zone

NW Set

Distance East of Omega Site (ft)

Figure 2.3.14. Variation of fracture strike from W to E along a portion of Los Alamos Canyon. This plot shows average krieged values for all fractures and for the NW and NE sets individually. Note that the angle between fracture sets remains fairly constant at ~60°, except over the fault (fracture) zone, where the average value varies antithetically. Figure 2.3.14. Variation of fracture strike from W to E along a portion of Los Alamos Canyon. This plot shows average krieged values for all fractures and for the NW and NE sets individually. Note that the angle between fracture sets remains fairly constant at ~60°, except over the fault (fracture) zone, where the average value varies antithetically.

W   50'   Bandelier Tuff: East Jemez Road   E
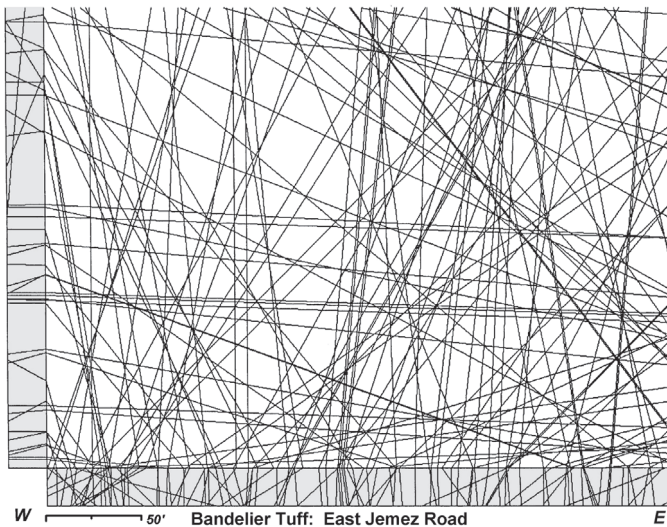
Figure 2.3.15. Projection of fractures measured on an E-W section showing a more acute (rhombic) intersection where fractures are more closely spaced.

TABLE 2.3.3. FRACTURE DIP DATA

Fracture set	Number	Mean dip from vertical (°)	Standard deviation
All fractures	4940	78N	±26
NE	2820	77N	±26
N	1447	69N	±26
S	393	67S	±20
NW	2120	81N	±25
N	1165	71N	±23
S	310	60S	±23
Background (west)	1085	81N	±29
NE	557	77N	±32
NW	528	84N	±27
Fault zone	933	78N	±34
NE	527	76N	±33
NW	406	79N	±36
Background (east)	1297	82N	±26
NE	756	81N	±26
NW	541	83N	±26

TABLE 2.3.4. FRACTURE APERTURE DATA

Fracture set	Number	Mean aperture (cm)	Standard deviation
All Fractures	4940	0.95	±1.73
NE	2820	0.98	±1.86
NW	2120	0.91	±1.46
Background (west)	1085	0.65	±0.92
NE	557	0.69	±0.97
NW	528	0.62	±0.85
Fault zone	933	0.97	±1.54
NE	527	0.94	±1.37
NW	406	1.18	±1.76
Background (east)	1297	0.69	±0.74
NE	756	0.69	±0.77
NW	541	0.67	±0.72

Fracture Fill

Apparently physically continuous with soils on the tuff surface, fracture fill materials exist downward 3–15 m below the surface, below which fractures are open. These materials are dominantly composed of illuviated clays (smectite, illite, and kaolinite) derived from weathering of the tuffaceous soils that infiltrated open fractures, hence they are pedogenic. Precipitated calcite, derived from soil water, fills in pores and shrinkage cracks in clays, forming vertical laminae common in fracture fill materials where apertures are greater than several centimeters. The fill material also includes minor amounts of mineral grains and fragments from the tuff. A crude zonation of fill materials is evident in some places where weathered tuff and clay minerals are most common near the fracture faces and infiltrated soil detritus and calcite is more abundant in central portions of the filled zone (Figs. 2.3.19 and 2.3.20). Because of the pedogenic origin of fracture fill materials, fractures have been subjected to oxidizing effects of water infiltration. Oxidation alteration is manifested on fracture faces and tuff immediately adjacent to fractures, where a zone of alteration up to several centimeters thick is marked by iron-oxide staining (Fig. 2.3.21).

The Role of Cooling Fractures in Tectonic Displacement

Overall the character of fractures in the Bandelier Tuff indicates that their ultimate origin is tied to columnar jointing by cooling contraction of the tuff. However, tectonics may likely have played an important role in determining the substrate over which the tuff compacted, and, subsequently, by imparting stress upon the tuff that would ultimately be relieved by opening of these cooling fractures. This conclusion is supported by the increases

Overall, fracture average apertures range from 0.7 to 1.0 cm, but average fracture aperture in the tectonic zone increases to over 2.0 cm (Table 2.3.4).

Figure 2.3.17 shows variation in fracture aperture along Los Alamos Canyon. Over nontectonic regions, the average aperture fluctuates between 0.2 and 1.0 cm, but over fault zones, it can increase to over 3.0 cm where fracture density is also much higher. In general, fracture aperture increases with fracture dip such that nearly horizontal fractures are generally closed and vertical ones have well-developed apertures (Fig. 2.3.18), a relationship that supports the model that tuff cooling fractures accommodate horizontal strain.

Figure 2.3.16. E-W variation of fracture dips (measured from vertical) along Los Alamos Canyon. Considerable fluctuation of dips occurs over the fault zone, where dips tend to be less vertical.

Fracture Aperture Along Los Alamos Canyon
(OU - 1098)

Legend:
- (0.03) Smoothed
- Cumulative / 100 ft

Los Alamos Canyon Fracture Widths
(TA-21)

Legend:
- Fracture Density (100 ft interval)
- (0.02) Smoothed Fracture Widths (cm)

Labels: MDA-V, MDA-B, MDA-T, MDA-A, MDA-U

X-axis: Distance East of Omega Site (ft)
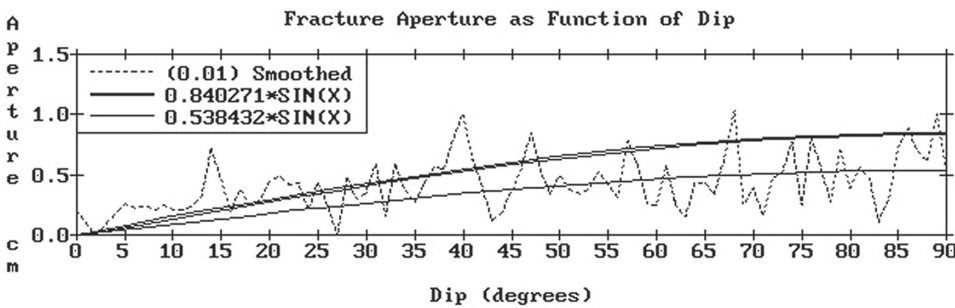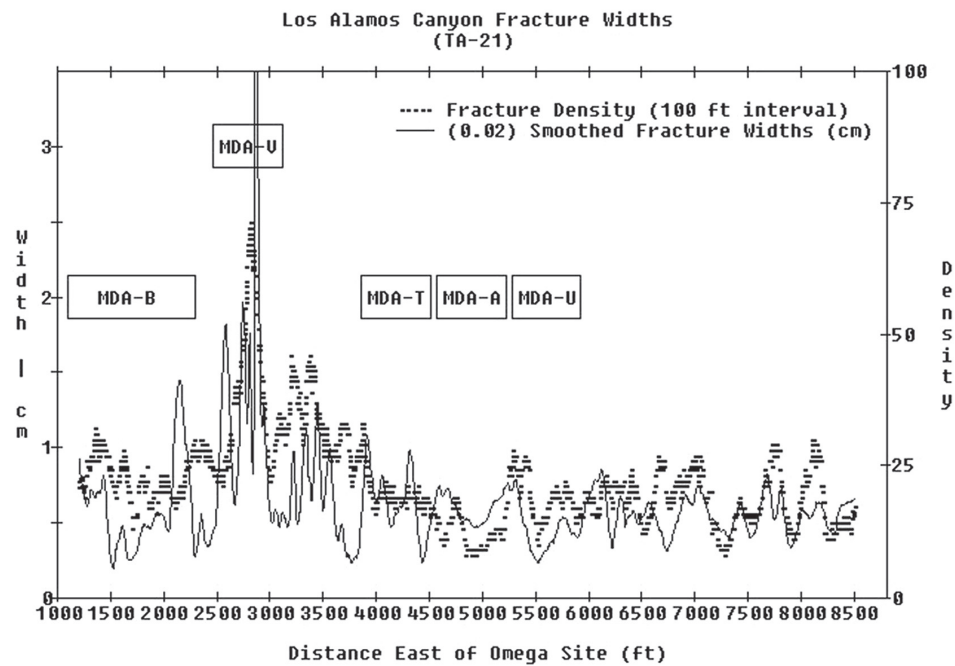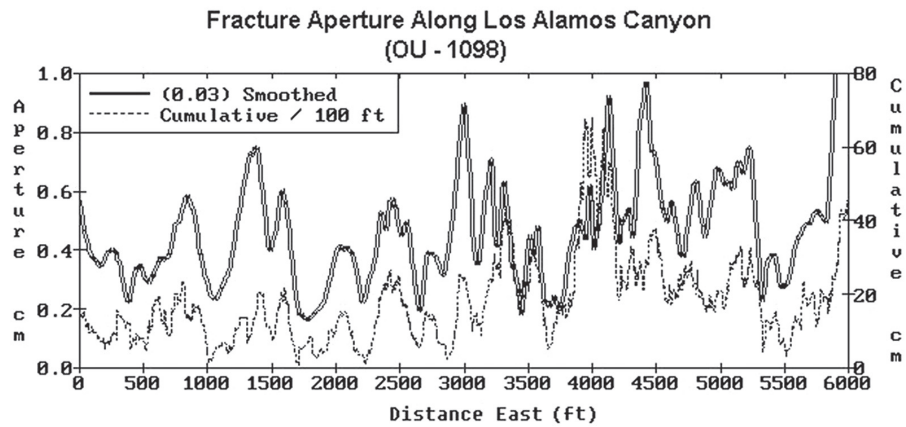
Figure 2.3.17. The top plot shows fracture aperture variation over a nontectonic region near Omega site in Los Alamos Canyon (3500 ft east). The bottom plot shows this variation further to the east over a branch of the Guaje Mountain fault (near MDA-V). Note in the lower part how fracture aperture mimics fracture density variation.

Fracture Aperture as Function of Dip

Legend:
- (0.01) Smoothed
- 0.840271*SIN(X)
- 0.538432*SIN(X)

X-axis: Dip (degrees)

Figure 2.3.18. Variation of fracture aperture with fracture dip. A sinusoidal function adequately expresses this variation.
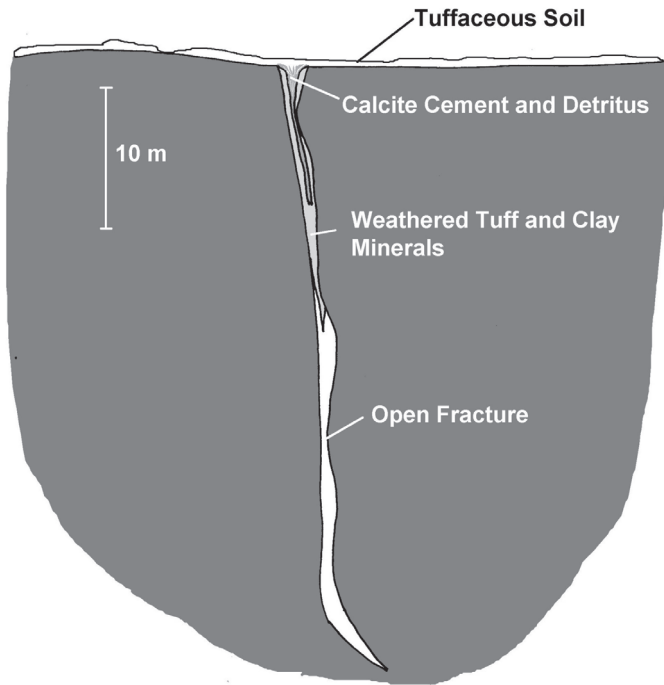
Figure 2.3.19. Schematic illustration of fracture fill materials for the Bandelier Tuff. Note the crude zonation of fill materials where weathered tuff and clay minerals dominate the fill near the fracture faces, and infiltrated calcite cement and soil detritus is more abundant in the central portions of the filling material.

of fracture linear density and average fracture aperture as well as the rotation of fracture orientation noted over fault zones.

Figure 2.3.22 is a schematic illustration of the role of tectonics in fracture orientation. When the tuff was emplaced, it ponded and was thicker in the canyons. During its cooling and compaction, the greatest vertical displacement of the tuff surface occurred in these canyons, concentrating tensional stresses along the canyon walls with cooling fractures developing parallel to the canyons. Another effect of tectonics was regional extensional stress (Aldrich et al., 1986), which influenced the orientation of cooling fractures as the tuff contracted during its cooling. This horizontal stress orientation resulted in an antithetic network of cooling fractures, separated by an angle of 60°–90°, centered on the direction perpendicular to the regional extension. The role of tectonic stresses is detailed by Walters (1996).

As noted already, traces of the Rendija Canyon and Guaje Mountain faults are mapped across the Pajarito Plateau. North of Los Alamos, these faults display from several to tens of meters of vertical offset in surface rocks, but south of Los Alamos Canyon, the surface offset is difficult to measure. There is some indication of the offset by changes in surface slope over the faults, but little, if any, notable vertical offset of the tuff. Hypotheses regarding these observations include that either the fault offset decreases to the south to be negligible in the area of fracture studies or that the tuff has acted as a concealing unit and has accommodated fault offset by incremental movement on cooling fractures spread out over a wide region above the
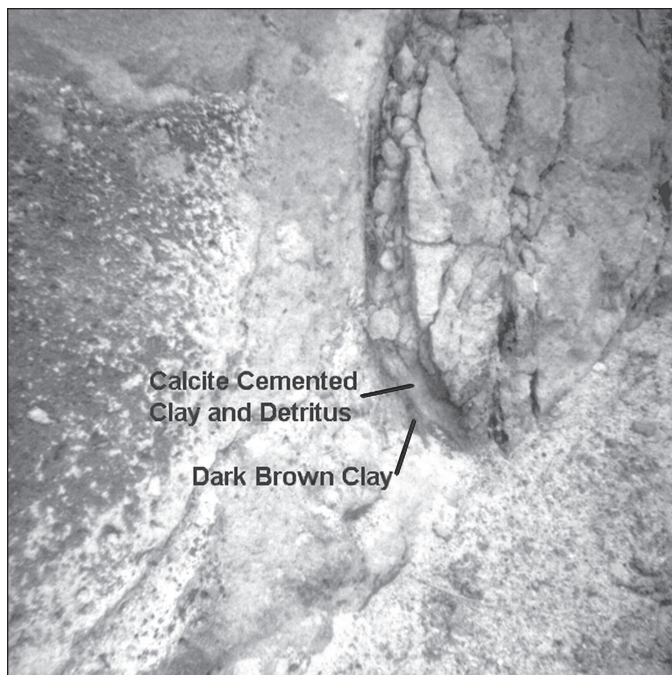
Figure 2.3.20. Close-up photograph showing the crude zonation of fracture fill materials. The calcite-cemented clay and detritus is a lighter color than the clay filling near the face of the fracture.
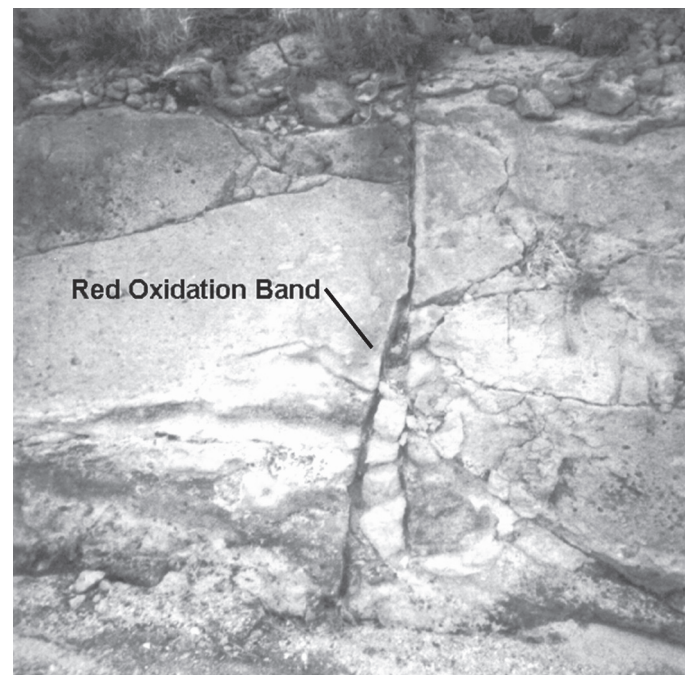
Figure 2.3.21. Reddish iron-oxidation stain along a fracture filled with 1–2 cm of clay and detritus; this fracture is only several feet below the tuff surface.

Canyon Wall Tensional Joints   **Tectonic-Influenced Joint Set**

Eroded Canyon
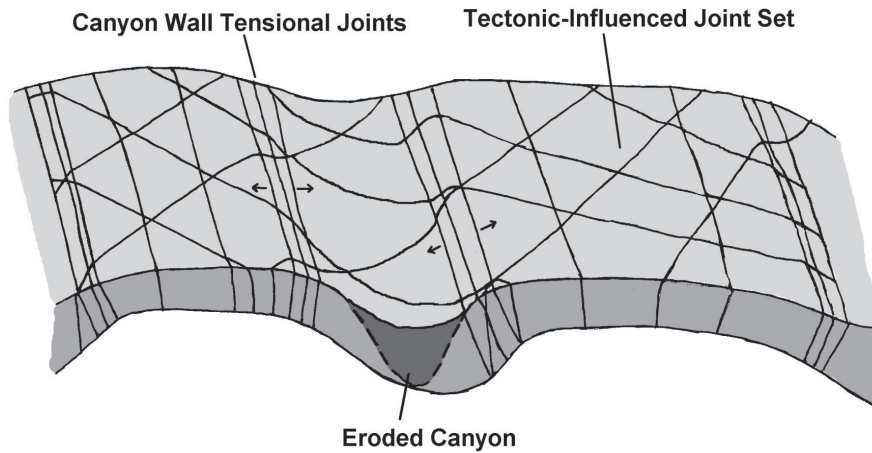
Figure 2.3.22. Schematic illustration of the effects of regional tectonism on the location and distribution of cooling fractures in a welded tuff.

fault. As demonstrated by the theoretical modeling and fracture characteristics noted herein, tuff cooling fractures accommodate horizontal strain by their aperture. By simple trigonometric projection, fracture aperture can be shown to accommodate vertical strain as well (Fig. 2.3.23).

By assuming that fracture aperture has developed by vertical displacement of the tuff in response to fault movement, a simple algorithm can be applied to all fractures that utilizes the fracture strike, dip, and aperture. Fractures striking perpendicular or nearly perpendicular to a fault trace do not produce any vertical displacement across a fault. However, fractures striking along or at some acute angle to a fault trace can produce vertical offset. Fractures dipping to the west produce down-drop to the east, whereas fractures dipping easterly produce down-drop to the west. The amount of down-drop is a function of fracture dip angle and aperture. By applying this trigonometric algorithm to a fracture profile that crosses a fault zone, one can see the potential vertical offset the fault has produced.

Figure 2.3.24 shows an example for a portion of Los Alamos Canyon cut by the trace of the Guaje Mountain fault. Hypothetical fracture vertical displacement is shown as sum of individual fracture displacement (negative values are west-side-down, and positive values are east-side-down) for 100 ft intervals centered on each fracture. By smoothing these data, fracture displacement is negligible (<10 cm) along most of the profile except over the fault zone, which extends ~1000 ft, from 3400 to 4400 ft east. Because this fault is known to have produced down-throw to the west, one can view the cumulative vertical displacement by sequentially summing the displacements on each fracture from east to west. Figure 2.3.25 shows that over the Guaje Mountain fault zone, a total cumulative displacement of ~3 m down to the west occurs over a distance of 700 ft. West of this zone, the cumulative displacement changes little. Figure 2.3.26 shows the same kind of plot as that in Figure 2.2.25, except it is for a profile along Mortandad Canyon, where both the Rendija Canyon and Guaje Mountain fault traces project. In Figure 2.3.26, the western shoulder of the Guaje Mountain fault shows

nearly the same profile in Mortandad Canyon as is documented for Los Alamos Canyon in Figure 2.3.25.

DISCUSSION

Overall, cooling fracture characteristics appear to have a relationship to tectonic stresses and strains. When viewing the data sets for these fractures, the distribution of characteristics does not appear to have any discernible patterns—that is the strike, dip, and aperture of one fracture looks to be independent from that of the next fracture, and so on. However, after applying a trigonometric algorithm that considers strike, dip, and aperture, a pattern along a fracture traverse becomes apparent. If one assumes that this pattern does in fact reflect the cumulative vertical displacement along fractures, then one sees that fracture characteristics must not be randomly distributed, but can be related to tectonism, and furthermore, the pattern produced by this trigonometric relationship is reproducible at different locations. To be sure, this trigonometric pattern may be due to some other nontectonic process, but as of yet that explanation has not been explored.

75° Average Dip

3.1 cm Apparent Downdrop

0.8 cm Average Aaperture
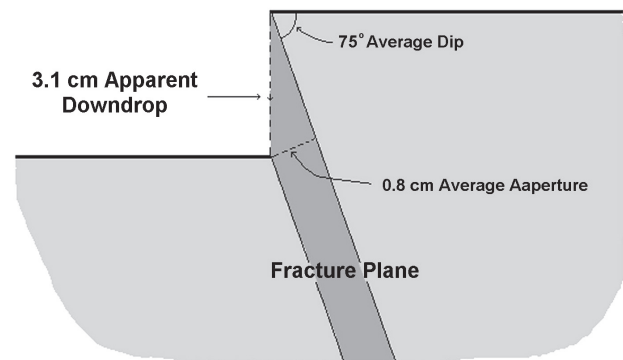
Fracture Plane

Figure 2.3.23. Schematic illustration of a dipping fracture with aperture produced by vertical displacement.

Calculated Vertical Displacement on Fractures
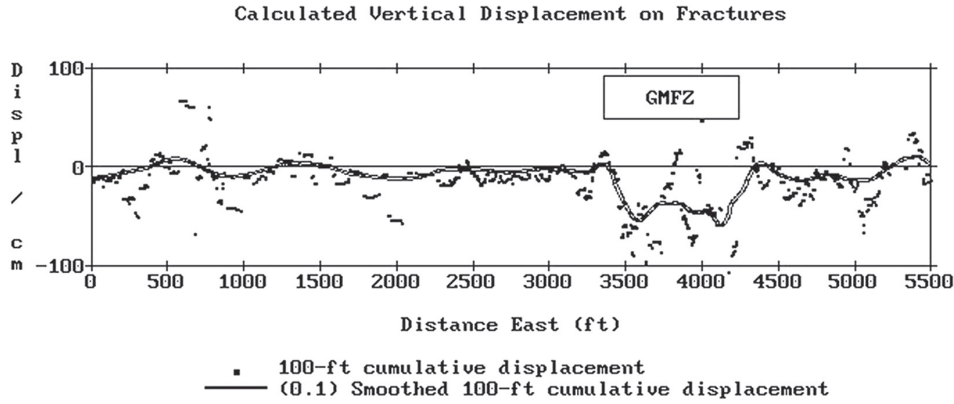
Figure 2.3.24. Plot of cumulative apparent fracture vertical displacement per 100 ft interval centered on each fracture. Note that cumulative displacement is nearly zero except over the Guaje Mountain fault zone, where it is negative (down to the west).

Calculated Cumulative Vertical Displacement on Fractures
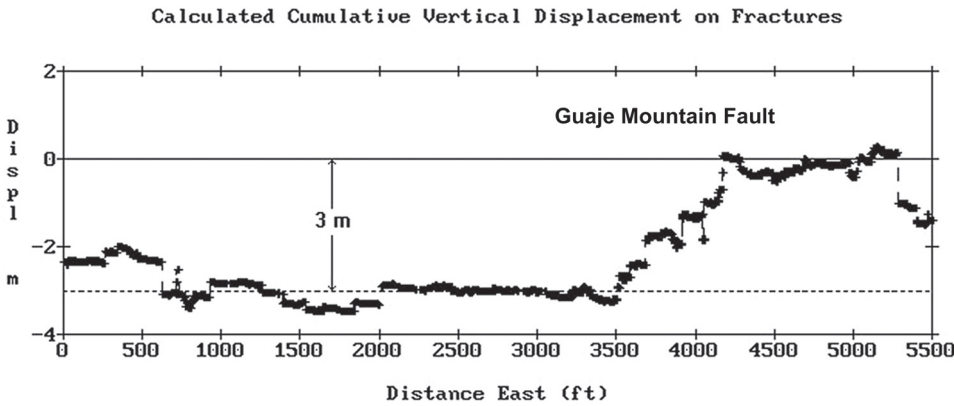
Figure 2.3.25. Cumulative apparent vertical displacement on fractures (summed from east to west), showing a 3 m downdrop over the Guaje Mountain fault zone (GMFZ).
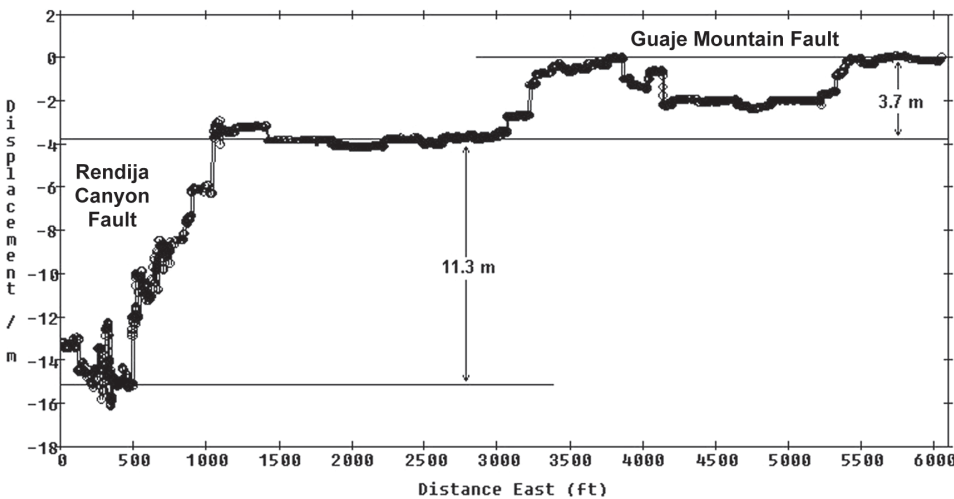
Figure 2.3.26. Similar to the plot in Figure 2.3.25, this cumulative apparent fracture displacement profile is for Mortandad Canyon where both Rendija Canyon and Guaje Mountain fault traces cross. The west shoulder of the Guaje Mountain fault shows a very similar offset and profile as it does in Los Alamos Canyon, depicted in Figure 2.3.25.

One may ask why cooling fractures are more abundant in fault zones if tectonic movement did not occur during the relatively short span of time during which cooling contraction occurred. The first answer to this question can be given for the circumstance that tectonism occurred prior to the tuff emplacement and cooling. In that case, there is a likelihood that the tuff was emplaced over a fault scarp, and differential compaction over the fault scarp might have concentrated stresses, requiring more fractures to incrementally accommodate the strain. A second answer lies in the fact that not all cooling fractures are equally well developed, such that many might have developed only a plane of minute dislocation or weakness without visible breakage, and some may have been reannealed during the welding process. In such circumstances where tectonic displacement occurs after cooling contraction, the added stress buildup in the tuff during faulting may cause these incipient or reannealed fractures to open up and become visible.

CONCLUSIONS

Welded tuffs develop fractures (joints) during cooling contraction that occurs after emplacement of the tuff. Best developed in welded zones, these fractures can extend throughout the entire thickness of tuff. Fracture spacing is on the order of meters and is smallest where cooling occurred rapidly and/or where the tuff has been faulted. Though dominantly vertically oriented, horizontal and plumose joint sets do form where cooling is influenced by substrate irregularities and fumarolic processes. It is typical to find fractures with apertures up to 1 cm or more. These apertures may be filled by clay minerals and detritus, especially in locations within several meters of the surface.

Fracture characteristics of strike, dip, and aperture may appear to be randomly distributed from field observations; however, there is a possibility that a stochastic relationship between these characteristics exists because of preexisting topographic fabric and postemplacement tectonic stresses.

The importance of tuff fractures is greatest in areas where a population center and associated industries exploit it for building material, aquifers, and waste disposal. Under saturated conditions, fractures promote infiltration of meteoric water and contaminants that may be placed at the surface or within the tuff, leading to widespread contaminant dispersal. Fractured tuffs can also display considerable slope instability near canyon walls by mass wasting associated with block falls. On the other hand, fractured tuffs display features that make them good aquifers where they are below the water table. In this setting, they are good hosts for geothermal reservoirs in areas of high heat flow. Also, saturated conditions may lead to rapid alteration of tuffs, such that fractures become sealed by zeolites and other secondary minerals. In this situation, fractured tuffs become aquitards.

ACKNOWLEDGMENTS

REFERENCES CITED

Aldrich, M.J., Jr., Chapin, C.E., and Laughlin, A.W., 1986, Stress history and tectonic development of the Rio Grande Rift, New Mexico: Journal of Geophysical Research, v. 91, p. 6199–6211.

Barton, C.C., and Larsen, E., 1985, Fractal geometry of two-dimensional fracture networks at Yucca Mountain, southwestern Nevada, *in* Proceedings of the International Symposium on Fundamentals of rock joints: Bjorkliden, Sweden, International Symposium Proceedings, p. 77–84.

DeGraff, J.M., and Aydin, A., 1993, Effect of thermal regime on growth increment and spacing of contraction joints in basaltic lava: Journal of Geophysical Research, v. 98, p. 6411–6430.

Fisher, R.V., and Schmincke, H.-U., 1984, Pyroclastic rocks: Berlin, Springer-Verlag, 472 p.

Francis, P., 1993, Volcanoes a planetary perspective: New York, Oxford University Press, Inc., 443 p.

Fuller, C.M., and Sharp, J.M., Jr., 1992, Permeability and fracture patterns in extrusive volcanic rocks: Implications from the welded Santana Tuff, Trans-Pecos, Texas: Geological Society of America Bulletin, v. 104, p. 1485–1496, doi: 10.1130/0016-7606(1992)104<1485:PAFPIE>2.3.CO;2.

Kolbe, T., Sawyer, J., Springer, J., Olig, S., Reneau, S., Hemphill-Haley, M., and Wong, I., 1995, Evaluation of the potential for surface faulting at TA-63, draft final report: Oakland, California, Woodword-Clyde Federal Services, unpublished report.

Lawn, B.R., and Wilshaw, T.R., 1975, Fracture of brittle solids: Cambridge, Cambridge University Press, 204 p.

Reneau, S.L., and Vaniman, D.T., 1998, Fracture characteristics in a disposal pit on Mesita del Buey: Los Alamos, Los Alamos National Laboratory Report LA-13539-MS, 21 p.

Ross, C.S., and Smith, R.L., 1961, Ash-flow tuffs: Their origin, geologic relations, and identification: U.S. Geological Survey Professional Paper 366, 81 p.

Vaniman, D., and Chipera, S., 1995, Mesa-penetrating fractures, fracture mineralogy, and projected fault traces at Pajarito mesa, *in* Geological site characterization for the proposed mixed waste disposal facility, Los Alamos National Laboratory: Los Alamos, Los Alamos National Laboratory Report LA-13089-MS, p. 71–86.

Vaniman, D., and Wohletz, K., 1990, Results of geological mapping/fracture studies, TA-55 area: Los Alamos, Los Alamos National Laboratory Seismic Hazards Memo EES1-SH90-17, 25 p.

Vaniman, D., and Wohletz, K., 1993, Reconnaissance geology of north-central LANL: Los Alamos, New Mexico, Los Alamos National Laboratory, Facility for Information Management, Analysis, and Display Map G101599, scale 1:7800.

Walters, M.C., 1996, Fracture analysis of the Bandelier Tuff, Pajarito Plateau, north-central Rio Grande Rift, New Mexico [MSc. thesis]: Fort Worth, Texas, Texas Christian University, 91 p.

Wohletz, K.H., 1995a, Measurement and analysis of rock fractures in the Tshirege Member of the Bandelier Tuff along Los Alamos Canyon adjacent to TA-21, *in* Broxton, D.E., and Eller, P.G., eds., Earth science investigations for environmental restoration—Los Alamos National Laboratory Technical Area 21: Los Alamos, Los Alamos National Laboratory report LA-12934-MS, p. 19–31.

Wohletz, K.H., 1995b, Fracture characterization of the DP Tank Farm: Los Alamos National Laboratory Environmental Restoration Technical Communication, Los Alamos National Laboratory, August 1995, 13 p.

Wohletz, K.H., 1996, Fracture characterization of the Bandelier Tuff in OU-1098 (TA-2 and TA-41): Los Alamos, Los Alamos National Laboratory Report LA-13194-MS, 19 p.

Wohletz, K.H., 1998, Fracture characterization along a portion of Mortandad Canyon: Los Alamos National Laboratory Environmental Restoration Technical Communication, Los Alamos National Laboratory, September 1998, 22 p.